

Experimental study of four-wave mixing based on a quantum dot semiconductor optical amplifier

Tokhmetov Akylbek, Tussupov Akhmet, Tanchenko Liliya

Department of Information Systems, L. N. Gumilyov Eurasian National University, Astana, Kazakhstan

Article Info

Article history:

Received Sep 29, 2022

Revised Feb 11, 2023

Accepted Feb 27, 2023

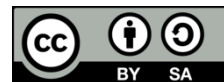
Keywords:

Four-wave mixing
Nonlinear optical devices
Optical signal processing
Quantum dots
Semiconductor optical amplifiers

ABSTRACT

The article is devoted to the study of four-wave mixing (FWM) in a semiconductor optical amplifier with quantum dots (QD-SOA). Experimental measurements of FWM signals are characterized in nonlinear media of GaAs-based QD-SOA with gain in the 1,550 nm region. Theoretical part of nonlinear effect of FWM is studied and important all-optical communication applications are listed. Experimental studies of a four-wave system are described and an analysis of FWM signals is given for various input powers of pump signals and injection currents. The devices are compared in terms of such parameters as conversion efficiency and signal-to-noise ratio. The results of the study made it possible to reveal the possibility of the effect of FWM signals on useful signals in channels with spectral division multiplexing wavelength division multiplexing (WDM) in the downstream and upstream in a semiconductor optical amplifier. Based on the experimental results, it was concluded that FWM does not affect adjacent channels of WDM signals and does not generate additional optical noise when scaling the WDM gigabit passive optical network (GPON) up to 60 km using semiconductor optical amplifiers (SOAs).

This is an open access article under the [CC BY-SA](https://creativecommons.org/licenses/by-sa/4.0/) license.



Corresponding Author:

Tokhmetov Akylbek

Department of Information Systems, L. N. Gumilyov Eurasian National University

11 Pushkin Street, building 2, Astana-010008, Kazakhstan

Email: tohmetovakylbek@gmail.com

1. INTRODUCTION

Nowadays, the usage of nonlinear mechanism of semiconductor optical amplifiers (SOAs) in advanced communication systems has been growing rapidly. SOAs are the most promising candidates because of their special nonlinearity characters with a basic nonlinear photonic component. There are three major nonlinear effects based on SOA: cross-gain modulation (XGM), cross-phase modulation (XPM) and four-wave mixing (FWM).

FWM in a SOA is a third order nonlinear effect, which has various potential applications in high-speed optical communication systems. This effect consists in the fact that in case of two (at least) different frequency beams ω_1 and ω_2 ($\omega_2 > \omega_1$) propagate together in a nonlinear medium, then modulation of the refractive index occurs at difference frequencies, which leads to the appearance of two additional frequency components $2\omega_1 - \omega_2$ and $2\omega_2 - \omega_1$. Similar processes occur when three (or more) incident waves exist. At the same time, the matching of the values of frequencies and wave vectors of all waves should be ensured [1]–[3].

Application of FWM in SOA has been widely demonstrated to all-optical devices, such as all optical wavelength conversion [4], all-optical pulse generation [5] optical samplers [6], optical multiplexers/demultiplexers [7], [8], optical phase conjugators [9] and 2R all-optical regenerator [10], [11] which are

expected to be used in optical communication systems. During the past few years nanostructural semiconductors are studied deeply. Electron's environment dimensions reduction or confining electrons (or holes) in active region leads to behavioral changes in semiconductor and invention of new types of SOAs such as quantum-wells, quantum-wires and quantum dots. Quantum dot semiconductor optical amplifiers (QD-SOAs) have been developed in order to overcome most of the limitations of conventional bulk or quantum-well SOAs. Indeed, the semiconductor structures with zero dimensionality in the "QD-SOA" medium region were expected to spread an atomic behavior to the electrons in the conduction band, which benefits in forecasting of several improved features such as fast gain recovery, reduced thermal dependence, broader amplification band and small or zero linewidth enhancement factor.

2. METHOD

2.1. Four-wave mixing theory

FWM is an effect which occurs in nonlinear medium with third-order susceptibility $\chi^{(3)}$ [12], [13]. This nonlinear phenomenon occurs when two optical fields at different frequencies interacts with each other and generates two unique optical fields at different frequencies. Optical properties are described by acceleration of dipole moments or polarization $P(t)$ in media when an optical field $E(t)$ interacts with it. Power series in the optical field $E(t)$ expresses polarization $P(t)$ in (1) [14].

$$P(t) = \varepsilon_0 [\chi^{(1)}E(t) + \chi^{(2)}E(t)^2 + \chi^{(3)}E(t)^3 \dots] \quad (1)$$

Where, $E(t)$ is the electric field; ε_0 is the vacuum permittivity. This equation consists of two parts: linear $P_L = \varepsilon_0 \chi^{(1)}E$, with the linear susceptibility $\chi^{(1)}$; and nonlinear part with second- $\chi^{(2)}$ and third- $\chi^{(3)}$ order nonlinear optical susceptibility and so on. Maxwell wave equation in nonlinear medium has a form of (2) [15].

$$\nabla^2 E - \frac{n^2}{c^2} \frac{\partial^2 E}{\partial t^2} = \frac{4\pi}{c^2} \frac{\partial^2 P_{NL}}{\partial t^2} \quad (2)$$

Where n is linear refractive index and c is the speed of light in vacuum. The polarization P_{NL} associate with nonlinear response drives the electric field E . This equation depicts that when it does not equal to zero, then charges accelerate, and these charges generate an electromagnetic radiation. Time-varying polarization can act as the source of new components of the electromagnetic field [16]. The third-order susceptibility $\chi^{(3)}$ gives rise to all nonlinear effects. The induced nonlinear polarization due to $\chi^{(3)}$ is expressed as (3),

$$P_{NL}^{(3)}(t) = \varepsilon_0 \chi^{(3)} E(t)^3 \quad (3)$$

where, $E(t)$ is the electric field which is made up of several different frequency components; $P_{NL}^{(3)}(t)$ is induced nonlinear polarization; $\chi^{(3)}$ is the third-order susceptibility. This fourth-rank tensor describing FWM has up to 81 independent components [17]. Two optical fields with different frequencies at ω_1 and ω_2 , which are also referred as pump and signal (probe) beams, are injected into nonlinear medium. The pump signal has up to 10 dB higher power than the signal power $|E_1|^2 > |E_2|^2$ which is shown in Figure 1.

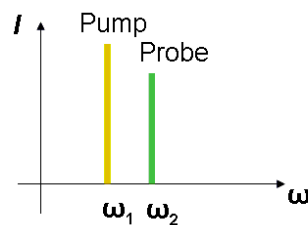


Figure 1. Input pump and signal power spectrum

Due to nonlinearities in the atomic response of the device, each atom develops an oscillating dipole moment which contains a component with " $\omega_1 + \omega_2$ " sum-frequency. The second-order susceptibility is dominated by carrier density modulation for small detuning between pump and probe due to the beating between the pump and the signal, so the polarization is given by the equation [18].

$$P = \epsilon_0 \frac{\partial \chi^{(n)}}{\partial n} \Delta n E \tag{4}$$

Where, Δn is the carrier density modulation. The beat frequency as shown in Figure 2 is a harmonic oscillation with a slowly varying amplitude that occurs during the interaction between the radiation of the pump ω_1 and the signal ω_2 propagating in the same direction (or between the signal ω_2 and the pump ω_1). This beat frequency is relatively small compared to ω_1 and ω_2 . It is expected that the carrier density will be modulated by the beat frequencies $\Delta\omega$ in (5) [19].

$$\Delta\omega = \omega_1 - \omega_2 \text{ and } \Delta\omega = \omega_2 - \omega_1 \tag{5}$$

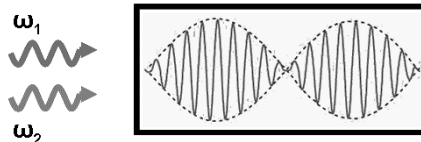


Figure 2. Modulation of the carrier density at the beat frequency

Modulation of the carrier density at the beat frequency $\Delta\omega$ of the pump and signal waves creates gain and index gratings. The number of carriers of the carrier density creates carrier density modulation which therefore creates refractive index modulation. Diffraction of the pump wave ω_1 at this dynamic grating generates a conjugate wave at $2\omega_1 - \omega_2$, also the signal wave ω_2 generates a conjugate wave at $2\omega_2 - \omega_1$ as shown in Figure 3.

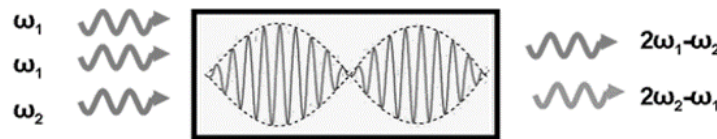


Figure 3. Generation of new waves

Figure 4 shows the energy-level diagram of photon description of FWM. These two conjugated waves differentiated as FWM red signal as shown in Figure 4(a) for $2\omega_1 - \omega_2$, for lower energy $E_1 = \hbar\omega_1$ (while $\omega_2 < \omega_1$) and FWM blue signal as shown in Figure 4(b) for $2\omega_2 - \omega_1$ for higher energy $E_2 = \hbar\omega_2$. As in all photon excitation processes, FWM must conserve energy and momentum.

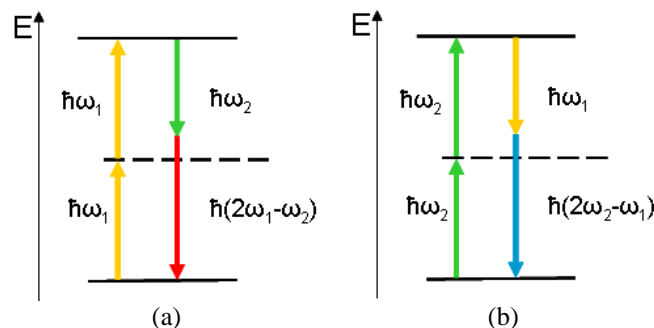


Figure 4. Energy-level diagram of photon description of FWM (a) energy conservation for FWM red signal and (b) energy conservation for FWM blue signal

The law of conservation of momentum necessitates phase matching, $\Delta k = 0$. To obtain constructive interference required for FWM, a phase matching between incident and generated photons is in (6) [19].

$$\begin{aligned}
 k_1 + k_1 - k_2 &= k_{FWM} \\
 E_1 + E_1 &= E_2 + E_{FWM} \\
 \hbar\omega_1 + \hbar\omega_1 &= \hbar(2\omega_1 + \omega_2)
 \end{aligned} \tag{6}$$

where, $k_i(i=1, 2, FWM)$ is phase vector (or wave vector):

$$k_i = \frac{n_i\omega_i}{c} \tag{7}$$

where, n_i represents the refractive index appropriate to the state of the ω_i . Figure 4(a) illustrates the energy conservation for FWM red signal. Here, two photons at $E_1=\hbar\omega_1$ with the same properties of frequency, phase and direction, strikes an atom of nonlinear oscillation at the same time. Electron in the atom will be excited from lower-energy state (valence band) to high energy state (conduction band). The energy of this state is the sum of the energies of the two incident photons E_1 . The high-energy state may be a real energy state, or a “virtual state” (dash line) of energy close to that of a real state. Then emitting a photon drops the energy to another virtual state, which is close to intermediary real state. This photon will be coherently interacted with third incident photon, at ω_2 frequency, with energy $E_2=\hbar\omega_2$. Then second generated new photon dropping from virtual state to ground state is shifted to $2\omega_1-\omega_2$ frequency, which is conjugated a wave. For generation a photon with $2\omega_2-\omega_1$ frequency the above process is repeated for two photons with frequency ω_2 (photon energy $E_2=\hbar\omega_2$) and one photon with frequency ω_1 (photon energy $E_1=\hbar\omega_1$) as shown in Figure 4(b). The spectral form of pump, signal and generated FWM signals are looking like in Figure 5.

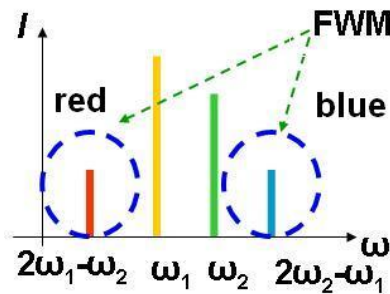


Figure 5. Spectral diagram of pump, signal and generated FWM signals

The power of FWM signals depends on powers of pump P_p at ω_1 frequency and on signal power P_s at ω_2 frequency. The intensity of the FWM red signal at $2\omega_1-\omega_2$ frequencies and FWM blue signal at $2\omega_2-\omega_1$ frequencies is proportional to (8) [20].

$$\begin{aligned}
 P_{FWM,red} &\propto P_p^2 P_s \\
 P_{FWM,blue} &\propto P_p P_s^2
 \end{aligned} \tag{8}$$

Nonlinear materials, for our case SOAs play big role in amplifying input pump and signal powers and generating FWM signals. The intensity of FWM signals is proportional to the gain of SOA [20].

$$\begin{aligned}
 I_{FWM} &\approx G^3 - G \\
 G &= \exp(\Gamma gL)
 \end{aligned} \tag{9}$$

Where, G is total gain of SOA, Γ is the confinement factor; g is material gain; and L is amplification length. SOAs with an active region on quantum dots (QD-SOA) have a localization of carriers in zero-dimensional space. Quantum dots are realized as coherent-stressed, defect-free islands in self-organized epitaxial growth of heterostructures of inconsistent semiconductors [21]. The time characteristics of the QD-SOA make it promising for use in technologies with a speed of 1 Tbit/s [22]. The gain medium in the QD-SOAs demonstrates unique properties, such as ultrafast gain recovery in the order (~ 1 ps) [23], significant spectral gain width (~ 120 nm) [24], high gain (>25 dB) [25], low noise factor (>5 dB) [26], the ability to work without cooling [27], high dynamic range for input power, high stability for pulsating traffic [28], relative polarization insensitivity [29].

2.2. FWM signal description parameters

The spectral image of the FWM signals, which are generated by the pump and wanted signal emissions, is shown in Figure 6. FWM signals for high frequencies (or short wavelengths) were designated as FWM (blue). And FWM signals for low frequencies (or long wavelengths) were designated as FWM (red).

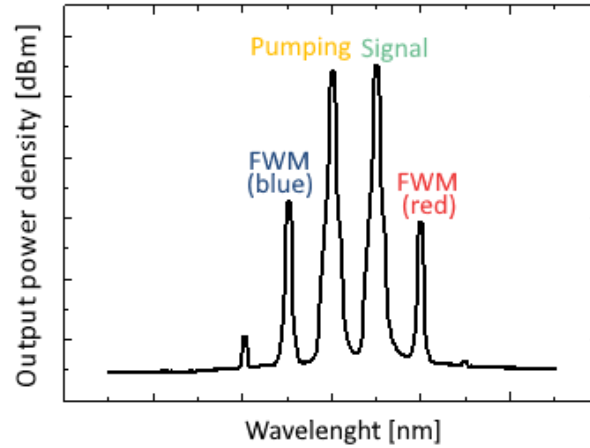


Figure 6. Spectral image of FWM signals

Conversion efficiency η is one of the most important parameters for describing FWM signals. The conversion efficiency is defined as the ratio of the FWM signal output power to the signal input power [30].

$$\eta = 10 \cdot \log \frac{P_{FWM}}{P_{signal}}$$

$$\eta = P_{FWM} - P_{signal} [dB] \quad (10)$$

The conversion efficiency shows its dependence on the initial parameters, such as the input power of the pump signal and the useful signal, as well as the wavelength (or frequency) and device parameters, such as the gain, the length of the SOA, and the constant gain of the substance. Another parameter as important as conversion efficiency for successful FWM is the optical signal to noise ratio. The main source of noise in an optical amplifier is amplified spontaneous emission (ASE). Due to the wide bandwidth, ASE is similar to the background noise of a conventional audio amplifier. The optical signal to noise ratio (OSNR) [dB] is a measure of the ratio of signal power to noise power in an optical channel [31].

$$OSNR = \frac{P_{signal}}{P_{noise}}$$

$$OSNR = P_{signal} - P_{noise} [dB] \quad (11)$$

Where, P_{signal} is the signal power; P_{noise} is the ASE noise power. Amplified spontaneous emission (ASE) noise is an inevitable spontaneous process that occurs in the active region of the SOA. The number of carriers providing optical amplification is reduced by the process of spontaneous emission of photons. The power of the ASE noise spectral density is approximately proportional to the gain of the amplifier [32].

2.3. Experimental setup for measuring FWM signals

Figure 7 shows an experimental setup for generating and measuring FWM signals, which consists of two arms, the upper arm is designed to generate a continuous laser beam acting as a pump, and the lower one is used to generate a signal wave. Both branches consist of lasers, attenuators and polarization controllers. A tunable laser is used as a pumping laser, and a laser at a certain wavelength is used to generate a signal. The generated light waves are combined in a 3 dB connector (50:50). An additional attenuator (attenuator-3) is installed between the 50:50 and 99:1 connector and performs the power control function before the test device (QD-SOA). 99:1 connector integrated with wattmeters are designed to control the connection of the test device to the optical fiber. The output signals are monitored by an optical spectrum analyzer (OSA).

A QD-SOA was taken as a test device. In this case, we used an optical amplifier based on an InAs/InP type connection. The amplifier parameters are shown in Table 1.

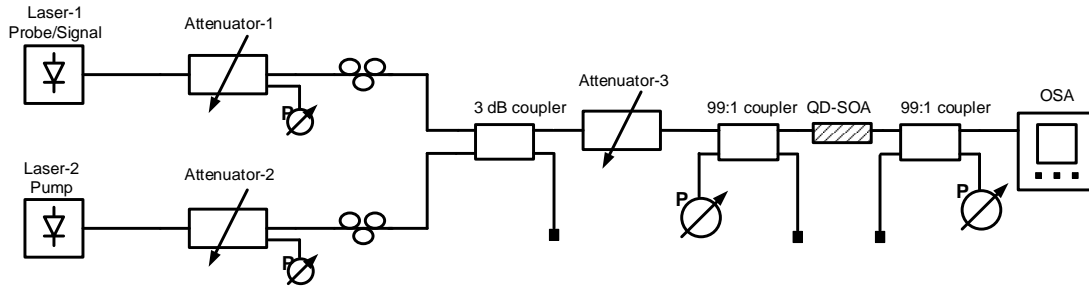


Figure 7. Experimental setup for measuring FWM signals

Table 1. Parameters of the optical amplifier for the experiment

Name	Active layer type	Operating wavelength range (nm)	Waveguide tilt angle (°)	Width (μm)	Length (mm)
Alcatel	quantum dots	1,550	7	1.5	2

3. RESULTS AND DISCUSSION

3.1. The main parameters characterizing the efficiency of SOAs

Important parameters characterizing the efficiency of SOAs are the gain and the coefficient of amplified spontaneous emission (ASE). Figure 8 demonstrates results of research of the gain dependence and ASE noise intensity on the input signal power and wavelengths. Figure 8(a) shows change dynamics in the QD-SOA gain depending on the input signal power in 1,540-1,560 nm wavelength range. The input power was measured directly during testing at the device entrance. The sample temperature set at 20 °C, the current injection into the QD-SOA was 200 mA.

It can be seen that at low input power levels, the gain is quite high. With an input power of -20 dBm, the gain (small signal gain) is 17-20 dB. Increasing the input power level to 0 dB reduces the gain to 8 dB. This is due to the fact that at high input power levels, the number of stimulated emission carriers is depleted, thereby reducing the electron concentration in the conduction band. The low concentration of electrons capable of stimulated emission is the main reason for the low gain. In addition, the obtained dependence of the gain on the signal wavelength showed that at short wavelengths the gain is greater than at long wavelengths. At 1,540 nm the gain was 20 dB, and at 1,560 nm the gain drops to 17 dB.

Figure 8(b) shows the ASE noise dependence on the wavelength at different values of the injection current. It can be concluded that the QD-SOA has a minimum ASE noise intensity of -52 dB at a 1,550 nm wavelength and with a 100 mA injection current. Along with an increase in the supplied injection current to 200 mA, the ASE noise intensity increases to -25 dB. During a further increase in the injection current, the intensity of the ASE noise rises, and the extremum of the noise intensity curve shifts: from long to short wavelength. The ASE noise intensity curves describe the behavior of the amplifier gain. The noise figure of QD-SOA is 10 dB, the polarization dependence is 2-5 dB.

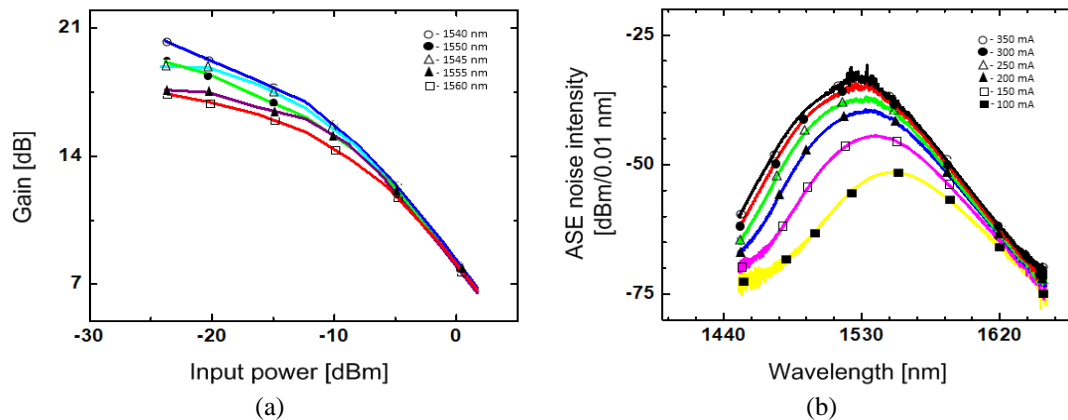


Figure 8. Dependences of the main parameters on the input signal power and wavelength (a) gain and (b) ASE noise intensity

3.2. Output power density, conversion efficiency and OSNR at various input pump powers

Figure 9 shows the dependence of the output powers of the pump, useful signal, FWM signals, and ASE noise on the input powers of the pump signals. The output power density curves were obtained for the input power range of pump signals from -10 dBm to +8 dBm with a wavelength of 1,550 nm and the useful signal input power of -1 dBm. The injection current was 200 mA, the sample temperature was 20 °C.

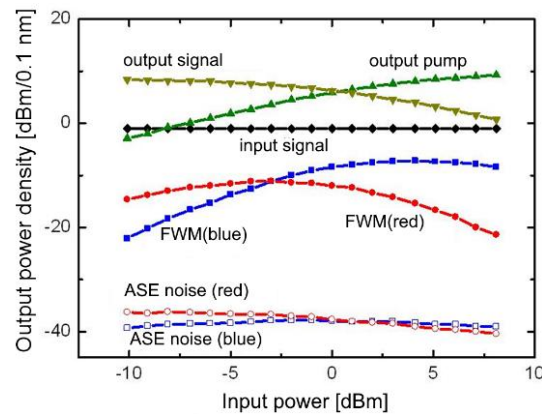


Figure 9. Output powers dependence of the pump signal, useful signal, FWM signals, and ASE noise on the input powers of the pump signals in a QD-SOA with an operating wavelength range of 1.5 μ m

It can be seen that the output pump power increases exponentially with an increase in the input pump power, while the output power of the useful signal, on the contrary, decreases. With an input pump power of -10 dBm, the output pump power is increased to -2 dBm, resulting in a gain of 7 dB. Simultaneously, the input signal with a constant power of -1 dBm is amplified to +9 dBm, which is a gain of 10 dB. The gain of the wavelength of 1,550 nm is 15 dB at an input power of -10 dBm, and 9 dB at -1 dBm. When the input pump power is increased to +8 dBm, the output pump power is increased to +10 dBm, i.e. the gain is 2 dB. With a further increase in the input power of the pump signal, the output power of the useful signal decreases to +1 dBm, and the gain increases by 2 dB. In addition, the output power curves of the pump signal and the wanted signal intersect at +6 dBm at 0 dBm of the input power of the pump signal, i.e. at this point the powers of the pump and useful signals are equal.

The emission of the pump signal and the useful signal in the QD-SOA generate FWM signals. The level of FWM signals depends on the pump power level. With an input pump power of -10 dBm and a useful signal power of -1 dBm, the power of the FWM signals for FWM (blue) is -22 dBm and FWM (red) is -14 dBm. As the pump input power increases, the power of the FWM (blue) signal increases and reaches its maximum of -7 dBm over the pump input power range from 0 to +7 dBm. As the input pump power is increased further, the FWM signal power (blue) gradually decreases to -8 dBm at a pump power of +8 dBm. As the input power of the pump signal is increased, the power of the FWM signal (red) increases and reaches its maximum of -12 dBm over the input power interval of the pump signal from -7 to -1 dBm. As the input pump power is further increased, the power of the FWM signal (red) gradually decreases to -21 dBm at a pump signal power of +8 dBm. The ASE noise that distorts the FWM signals has a power of about -28 dBm. From the obtained FWM signal curves, the FWM conversion efficiency parameter was calculated. The values presented in the experimental graphs as shown in Figure 10 were calculated using (11).

With input pump powers of -10 dBm and a signal of -1 dBm, the signal conversion efficiency of FWM (blue) is -21 dB, the signal conversion efficiency of FWM (red) is -12 dB. As the pump input power increases, the conversion efficiency of the FWM (blue) signal increases and reaches its maximum of -6 dB in the pump input power range from 0 to +7 dBm. As the input pump power is further increased, the conversion efficiency of the FWM (blue) signal gradually decreases to -7 dB at a pump power of +8 dBm.

The dynamics of the change in the conversion efficiency of the FWM signal (red) is similar. As the pump input power increases, the conversion efficiency of the FWM (red) signal increases and reaches its maximum of -10 dB in the pump input power range from -7 to -1 dBm. As the input pump power is further increased, the signal conversion efficiency of the FWM (red) gradually decreases to -20 dB at a pump power of +8 dBm. Figure 11 shows the OSNR as a function of input pump powers for input pump powers of -10 dBm and a wanted signal of -1 dBm. Initially, the OSNR of the FWM signal (blue) was 17 dB and the OSNR of the FWM signal (red) was 22 dB.

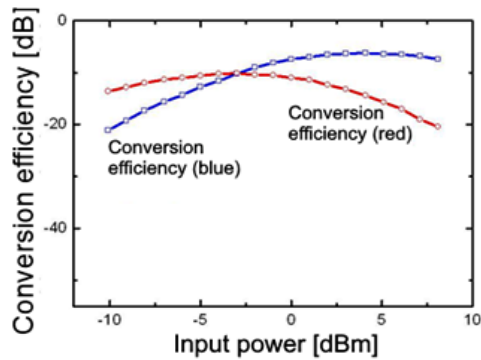


Figure 10. Conversion efficiency dependence on the input pump powers

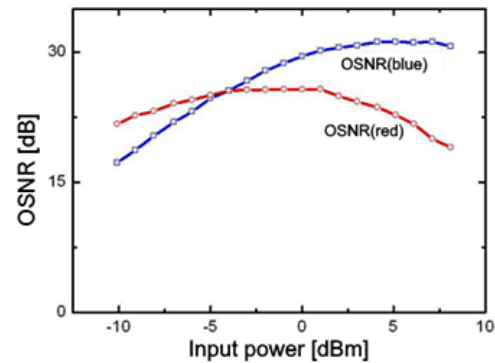


Figure 11. OSNR dependence on the input pump powers

As the input pump power increases, the OSNR of the FWM signal (blue) increases and reaches its maximum of 21 dB in the input pump power range from +2 to +7 dBm. With a further increase in the input pump power, the OSNR of the FWM signal (blue) gradually decreases and reaches 20 dB at a pump power of +8 dBm. As the input pump power increases, the OSNR of the FWM signal (red) increases and reaches its maximum of 26 dB over the input pump power interval from -4 to +1 dBm. With a further increase in the input pump power, the OSNR of the FWM signal (red) gradually decreases and reaches 19 dB at a pump power of +8 dBm.

3.3. Dependence of output powers of FWM signals, conversion efficiency and OSNR on pump and signal wavelength detuning

Figure 12 shows the results of studying the dependence of the FWM signal level, conversion efficiency and OSNR on the wavelength detuning. Figure 12(a) shows the power of the FWM signals as a function of the detuning between the pump and signal wavelengths. In this case, by a positive wavelength detuning we mean the detuning of the pump and signal lengths in an increasing direction with respect to the wavelength of the incoming pump radiation, and by a negative detuning, we mean a detuning in a decreasing direction with respect to the wavelength of the incoming pump radiation.

The initial pump input power is 0 dBm, the signal input power is -1 dBm. Wavelength detuning interval from ~0 to 8 nm. The injection current into the sample was 200 mA, the sample temperature was 20 °C. The dynamics of changes in FWM signals depending on the wavelength detuning have the following form. With a positive detuning of ~0 nm, the power of the FWM signal (blue) is -4 dBm. As the detuning increases to 1 nm, the power of the FWM signal (blue) drops rapidly to -17 dBm. As the detuning is further increased to 8 nm, the power of the FWM (blue) signal is reduced to -20 dBm. With a negative detuning of ~0 nm, the power of the FWM signal (blue) is -7 dBm. As the detuning increases to 1 nm, the power of the FWM signal (blue) drops rapidly to -19 dBm. As the detuning is further increased to 8 nm, the power of the FWM (blue) signal is reduced to -21 dBm.

With a positive detuning of ~0 nm, the power of the FWM signal (red) is -2 dBm. As the detuning increases to 1 nm, the power of the FWM signal (red) drops rapidly to -22 dBm. As the detuning is further increased to 8 nm, the power of the FWM signal (red) is reduced to -29 dBm. With a negative detuning of ~0 nm, the power of the FWM signal (red) is -1.2 dBm. As the detuning increases to 1 nm, the power of the FWM signal (red) drops rapidly to -22 dBm. As the detuning is further increased to 8 nm, the power of the FWM signal (red) drops to -27 dBm.

Figure 12(b) shows the dependence of the conversion efficiency of the FWM signals on the detuning of the pump and signal wavelengths. With a positive detuning of ~0 nm, the signal conversion efficiency of the FWM (blue) is -2 dB. As the detuning is increased to 1 nm, the conversion efficiency of the FWM (blue) signal rapidly drops to -16 dB. As the detuning is further increased to 8 nm, the conversion efficiency of the FWM (blue) signal is reduced to -29 dB. With a negative detuning of ~0 nm, the signal conversion efficiency of the FWM (blue) is -6 dB. As the detuning increases to 1 nm, the FWM (blue) signal conversion efficiency drops rapidly to -18 dB. As the detuning further increases to 8 nm, the conversion efficiency of the FWM (blue) signal drops to -20 dB.

With a positive detuning of ~0 nm, the signal conversion efficiency of the FWM (red) is -1 dB. As the offset increases to 1 nm, the FWM (red) signal conversion efficiency drops rapidly to -22 dB. With a further increase in detuning to 8 nm, the conversion efficiency of the FWM (red) signal is reduced to -28 dB.

With a negative detuning of ~ 0 nm, the signal conversion efficiency of the FWM (red) is -0.2 dB. As the offset increases to 1 nm, the FWM (red) signal conversion efficiency drops rapidly to -21 dB. As the offset is further increased to 8 nm, the conversion efficiency of the FWM (blue) signal is reduced to -26 dB.

Figure 12(c) shows the OSNR of the FWM signals as a function of the pump and signal wavelength detuning. With a positive offset of ~ 0 nm, the OSNR of the FWM signal (blue) is 42 dB. As the detuning is increased to 1 nm, the OSNR of the FWM signal (blue) rapidly drops to 22 dB. As the detuning is further increased to 8 nm, the OSNR of the FWM signal (blue) drops slightly to 20 dB. With a negative detuning of ~ 0 nm, the OSNR of the FWM signal (blue) is 40 dB. As the detuning is increased to 1 nm, the OSNR of the FWM signal (blue) rapidly drops to 22 dB. As the detuning is further increased to 8 nm, the OSNR of the FWM signal (blue) drops slightly to 20 dB.

With a positive detuning of ~ 0 nm, the OSNR of the FWM signal (red) is 44 dB. As the detuning is increased to 1 nm, the OSNR of the FWM signal (red) rapidly drops to 27 dB. As the detuning is further increased to 8 nm, the OSNR of the FWM signal (red) is reduced to 12 dB. With a negative detuning of ~ 0 nm, the OSNR of the FWM signal (red) is 45 dB. As the detuning is increased to 1 nm, the OSNR of the FWM signal (red) rapidly drops to 28 dB. As the detuning is further increased to 8 nm, the OSNR of the FWM signal (red) is reduced to 12 dB.

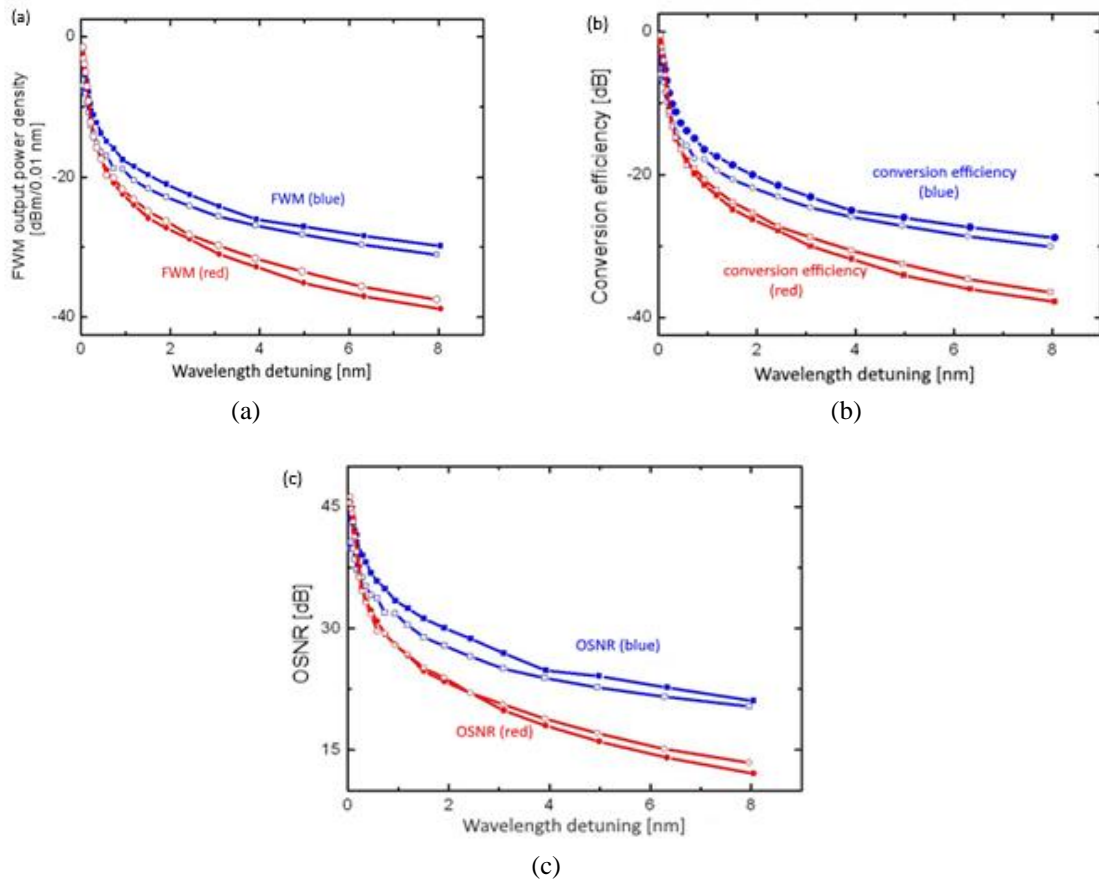


Figure 12. Dependencies of (a) FWM signal powers, (b) conversion efficiency, and (c) OSNR on wavelength tuning

4. CONCLUSION





This article discusses the main parameters for describing FWM signals, such as conversion efficiency, amplified spontaneous emission noise, and optical signal-to-noise ratio. An experimental setup for the of FWM signals behavior as a research stage is described. The experimental results are analyzed on the basis of the theory of stationary signals propagation in the infrared range. Various parameters were studied: such as the output power of the FWM signals, the conversion efficiency and the optical signal-to-noise ratio and their dependence on the input powers of the pump signals, the input powers of the useful signal, the injection currents, and the frequency detuning between the pump signals and the useful signal.

Based on experimental results, it was found that FWM does not affect adjacent channels of WDM signals and does not generate additional optical noise. This can be explained by the fact that the input power of the signal does not exceed the input saturation power of the SOA and the wavelength detuning between two useful WDM signals exceeds 6 nm. In the case of high input powers to a semiconductor optical amplifier and detuning less than 6 nm, the generated FWM signals will be superimposed on the useful signals as optical noise.





REFERENCES

- [1] R. Boyd, *Contemporary nonlinear optics*. Academic Press, 2012.
- [2] N. Bloembergen, *Nonlinear optics*, 4th Editio. World Scientific, 1996.
- [3] Y.-R. Shen, *Principles of nonlinear optics*. Wiley-Interscience, New York, NY, USA, 1984.
- [4] Rajni and A. Sheetal, "Optical wavelength converters based on four wave mixing in SOA-MZI configuration," *MATEC Web of Conferences*, vol. 57, May 2016, doi: 10.1051/mateconf/20165701017.
- [5] F. Li and A. S. Helmy, "All-optical pulse generation based on gain-induced four-wave mixing in a semiconductor optical amplifier," *Optics Letters*, vol. 38, no. 8, Apr. 2013, doi: 10.1364/OL.38.001241.
- [6] H. Kawaguchi and J. Inoue, "Four-wave mixing among subpicosecond optical pulses in a semiconductor optical amplifier and its applications to optical sampling," in *Physics and Simulation of Optoelectronic Devices VI*, Jul. 1998, doi: 10.1117/12.316698.
- [7] M. Saruwatari, "All-optical time-division multiplexing technology," in *Springer Series in Photonics*, Springer Berlin Heidelberg, 2001, pp. 338–375.
- [8] K. Uchiyama, S. Kawanishi, and M. Saruwatari, "100-Gb/s multiple-channel output all-optical OTDM demultiplexing using multichannel four-wave mixing in a semiconductor optical amplifier," *IEEE Photonics Technology Letters*, vol. 10, no. 6, pp. 890–892, Jun. 1998, doi: 10.1109/68.681520.
- [9] C. L. Janer and M. J. Connelly, "Optical phase conjugation technique using four-wave mixing in semiconductor optical amplifier," *Electronics Letters*, vol. 47, no. 12, 2011, doi: 10.1049/el.2011.0737.
- [10] E. A. M. Fagotto and M. L. F. Abbade, "Wavelength shift-free all-optical 2R regenerator based on four-wave mixing," in *2011 SBMO/IEEE MTT-S International Microwave and Optoelectronics Conference (IMOC 2011)*, Oct. 2011, pp. 679–683, doi: 10.1109/IMOC.2011.6169306.
- [11] M. U. Khan, A. J. Aljohani, A. Gulistan, and S. Ghafoor, "All-optical multi-wavelength regenerator based on four-wave mixing," *Optical Engineering*, vol. 60, no. 3, Mar. 2021, doi: 10.1117/1.OE.60.3.036102.
- [12] G. Agrawal, *Nonlinear fiber optics*. Elsevier, 2012.
- [13] R. W. Boyd, *Nonlinear optics*. Academic press, 2020.
- [14] C. Li, *Nonlinear optics: principles and applications*. Springer, 2018.
- [15] R. Fitzpatrick, *Maxwells equations and the principles of electromagnetism*. Laxmi Publications, Ltd., 2010.
- [16] Y. Okuno, K. Sugiyama, T. Hajikano, Y. Tomomatsu, K. Yoshizawa, and H. Tsuda, "Polarization diversity circuit using photonic crystal waveplates for 1.2- μm quantum dot semiconductor optical amplifiers," in *2018 Photonics in Switching and Computing (PSC)*, Sep. 2018, pp. 1–3, doi: 10.1109/PS.2018.8751259.
- [17] S. Hess, *Tensors for physics*. Springer, 2015.
- [18] F. Baronio *et al.*, "Second and third order susceptibilities mixing for supercontinuum generation and shaping," *Optical Fiber Technology*, vol. 18, no. 5, pp. 283–289, Sep. 2012, doi: 10.1016/j.yofte.2012.07.001.
- [19] G. P. Agrawal, *Applications of nonlinear fiber optics*. Elsevier, 2008.
- [20] M. J. Connelly, *Semiconductor optical amplifiers*. Boston: Kluwer Academic Publishers, 2002.
- [21] N. N. Ledentsov, V. M. Ustinov, D. Bimberg, J. A. Lott, and Z. I. Alferov, "Applications of quantum dots in semiconductor lasers," *International Journal of High Speed Electronics and Systems*, vol. 12, no. 1, pp. 177–205, Mar. 2002, doi: 10.1142/S0129156402001150.
- [22] P. Bhattacharya, D. Bimberg, and Y. Arakawa, "Special issue on optoelectronic devices based on quantum dots," *Proceedings of the IEEE*, vol. 95, no. 9, pp. 1718–1722, Sep. 2007, doi: 10.1109/JPROC.2007.900896.
- [23] T. Vallaitis *et al.*, "Slow and fast dynamics of gain and phase in a quantum dot semiconductor optical amplifier," *Optics Express*, vol. 16, no. 1, 2008, doi: 10.1364/OE.16.000170.
- [24] R. Brenot *et al.*, "Quantum dots semiconductor optical amplifier with a-3 dB bandwidth of up to 120 nm in semi-cooled operation," in *OFC/NFOEC 2008-2008 Conference on Optical Fiber Communication/National Fiber Optic Engineers Conference*, Feb. 2008, pp. 1–3, doi: 10.1109/OFC.2008.4528574.
- [25] T. Akiyama, M. Sugawara, and Y. Arakawa, "Quantum-dot semiconductor optical amplifiers," *Proceedings of the IEEE*, vol. 95, no. 9, pp. 1757–1766, Sep. 2007, doi: 10.1109/JPROC.2007.900899.
- [26] D. Bimberg, "Quantum dot based nanophotonics and nanoelectronics," *Electronics Letters*, vol. 44, no. 3, 2008, doi: 10.1049/el:20080074.
- [27] H. Wang *et al.*, "Temperature independent optical amplification in uncooled quantum dot optical amplifiers," in *OFC/NFOEC 2008-2008 Conference on Optical Fiber Communication/National Fiber Optic Engineers Conference*, Feb. 2008, pp. 1–3, doi: 10.1109/OFC.2008.4528575.
- [28] R. Bonk *et al.*, "Single and multiple channel operation dynamics of linear quantum-dot semiconductor optical amplifier," in *2008 34th European Conference on Optical Communication*, 2008, pp. 1–2, doi: 10.1109/ECOC.2008.4729375.
- [29] R. Bonk *et al.*, "1.3/1.5 μm QD-SOAs for WDM/TDM GPON with extended reach and large upstream/downstream dynamic range," 2009, doi: 10.1364/OFC.2009.OWQ1.
- [30] N. Yasuoka *et al.*, "Quantum-dot semiconductor optical amplifiers with polarization-independent gains in 1.5- μm wavelength bands," *IEEE Photonics Technology Letters*, vol. 20, no. 23, pp. 1908–1910, Dec. 2008, doi: 10.1109/LPT.2008.2004695.
- [31] F. D. Mahad, A. S. M. Supa'at, S. M. Idrus, and D. Forsyth, "Analyses of semiconductor optical amplifier (SOA) four-wave mixing (FWM) for future all-optical wavelength conversion," *Optik*, vol. 124, no. 1, pp. 1–3, Jan. 2013, doi: 10.1016/j.ijleo.2011.11.024.
- [32] L. Qiao and P. J. Vella, "ASE analysis and correction for EDFA automatic control," *Journal of Lightwave Technology*, vol. 25, no. 3, pp. 771–778, Mar. 2007, doi: 10.1109/JLT.2006.889665.





BIOGRAPHIES OF AUTHORS

Tokhmetov Akylbek     Candidate of Physical and Mathematical Sciences in the specialty “Computer Science and Information Systems”, Associate Professor of the Department of Information Systems at the L.N. Gumilev Eurasian National University, Nur-Sultan, Kazakhstan. He has published more than 90 articles in journals and conferences on various topics related to research in the field of telecommunications and computer systems. His research interests include the following areas: information and telecommunication systems, electronics and circuit engineering. He can be contacted at email: tohmetovakylbek@gmail.com.



Tussupov Akhmet     received the Diploma degree in automatic telecommunication from Almaty Institute of Power Engineering and Telecommunication, Kazakhstan, in 2005; M.S. degree in Electrical Engineering and Information Technology from University of Karlsruhe/Karlsruhe Institute of Technology, Germany, in 2009 and Ph.D. degree in Information systems from Eurasian National University, Nur-Sultan, Kazakhstan in 2022. Currently, he is an account manager in Hewlett-Packard Enterprise in Kazakhstan. His research interests include the following areas: information and communication technologies, business process management and information technology management. He can be contacted at email: tussupov@gmail.com.



Tanchenko Liliya     received a bachelor’s degree in engineering and technology in the specialty 5B070300-“Information systems” in 2015, an academic degree of a master of technical sciences in the specialty 6M070300-“Information systems” at the University “Turan-Astana” in 2016. Her research interests include the development of information and telecommunications systems. She can be contacted at email: tanchenkoliliya@gmail.com.